Optics Communications 336 (2015) 160–165

Contents lists available at ScienceDirect

Optics Communications

journal homepage: www.elsevier.com/locate/optcom

Shape based zonal wave-front reconstruction for arbitrary shape pupils

Zhaoliang Cao [a,*], Qing Qu [a,b], Yukun Wang [a], Huanyu Xu [a], Shaoxin Wang [a], Chengliang Yang [a], Li Xuan [a]

[a] State Key Laboratory of Applied Optics, Changchun Institute of Optics, Fine Mechanics and Physics, Chinese Academy of Sciences, Changchun 130033, PR China

[b] Graduate School of Chinese Academy of Sciences, Beijing 100039, PR China

ARTICLE INFO

Article history:
Received 2 September 2014
Received in revised form
26 September 2014
Accepted 30 September 2014
Available online 13 October 2014

Keywords:
Zonal method
Wave-front reconstruction
Arbitrary shape
Low time consumption
Iteration

ABSTRACT

Zonal method is widely used to reconstruct the wave-front. Up to now, the iterative algorithms have been used to reconstruct the arbitrary shape wave-front with high reconstruction accuracy. However, it has the shortcomings of long time consumption. To reduce the time delay, a shaped based method is proposed by adding the shape information into the geometry matrix. The simulated and experimental results indicate that the reconstruction accuracy of proposed method is similar to that of the iterative LS-based method, but the computation time of our method is 3 times less than that of the iteration method. Consequently, the high accuracy and low time consumption are simultaneously achieved with the proposed method.

1. Introduction

Shack–Hartmannwave-front sensors (S–H WFSs) are popularly used to measure the wave-front which is reconstructed with the slope data. The reconstruction method includes the model [1,2] and zonal modes. The zonal method contains Fried [3], Southwell [4] and Hudgin models [5]. The Fourier-transform (FT) based algorithms [6,7] and the least-squares (LS) based algorithms [3,4,8] were used to reconstruct the wave-front for zonal method. For both algorithms, the iteration method is considered to improve the reconstruction accuracy. Firstly, Southwell proposed Jacobi, Gauss-Seidel and Successive Over-relaxation (SOR) iterative linear LS methods for zonal wave-front reconstruction [4]. To improve the reconstruction accuracy, Bahk developed the SOR method with a Simpson iterator and used it in the FT-based algorithm [9]. Furthermore, the boundary problem was also considered by lots of researchers [8,10,11]. At first, the wave-front reconstruction is investigated for square or rectangular pupils [12,13]. However, in practice, the measured pupils always have different shapes and then, the wave-front reconstruction is researched for arbitrary shapes [8,14]. Roddier and Roddier proposed a Gerchberg-type iterative FT-based algorithm to reconstruct the arbitrary shape wave-front[15]. Similarly, Zou and Rolland utilized the Gerchberg-type iterative linear LS-based approach to estimate the any pupil wave-front[14,16]. Even if all the methods reconstructed the arbitrary shape wave-front with high accuracy, as the accurate solution is obtained with many times of iteration, the iterative algorithm consumes much calculation time. In the paper, based on the linear LS algorithm, we present a new simple method to reconstruct the wave-front for arbitrary shape with high accuracy and low time delay.

To demonstrate our method conveniently, the Southwell model is selected as an example in the paper.

2. Shape based least squares method for arbitrary shape wave-front reconstruction

2.1. Southwell model

Fig. 1 shows the Southwell configuration for measured wave-front slope superimposed on phase determination points. The grid points in the center present the phases to be estimated, the measured slopes are also in the center of the sub-regions.

The measured slopes are related to the estimated phases by the equations below [17]:

$$g_{xi} = \frac{1}{2h}\left[(\varphi_{i,j+1} + \varphi_{i+1,j+1}) - (\varphi_{i,j} + \varphi_{i+1,j})\right] \quad (1)$$

* Corresponding author.
E-mail address: caozlok@ciomp.ac.cn (Z. Cao).

http://dx.doi.org/10.1016/j.optcom.2014.09.076
0030-4018/

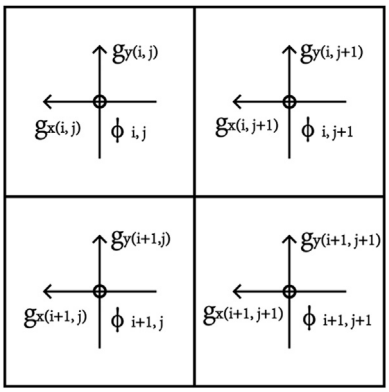

Fig. 1. Configuration of Southwell model.

$$\frac{1}{2}\left(g_{y(i+1,j)} + g_{y(i,j)}\right) = \frac{1}{h}\left(\phi_{i+1,j} - \phi_{i,j}\right). \tag{2}$$

Eqs. (1) and (2) can be written in matrix form [18]:

$$G = A\Phi, \tag{3}$$

where G is slope matrix, Φ is estimated phase matrix and A is geometry matrix. Therefore, the linear LS solutions of the estimated phase can be calculated by

$$\Phi = A^{+}G, \tag{4}$$

here the pseudo-inverse matrix A^{+} can be solved with singular value decomposition (SVD) method.

2.2. Revise of the geometry matrix

To reconstruct the arbitrary wave-front (Fig. 2), the geometry matrix A is expected to be revised with the shape information of the pupil. As shown in Fig. 2, the arbitrary shape wave-front is represented with •. Outside of the area, all the data are invalid. To add the shape information into the geometry matrix A, the mask matrix should be firstly constructed. 1 and 0 are used to represent inside or outside of the valid area. Assuming the numbers of the point are $n \times n$, the numbers of the data are $2 \times n \times n$ as one point has x and y dimensions. According to this, the mask matrix may be written as

$$M = \begin{bmatrix} p_1 \\ \vdots \\ p_{n^2} \\ p_1 \\ \vdots \\ p_{n^2} \end{bmatrix}, \tag{5}$$

where p represents the status of the point and it equals to 1 or 0 according to the point is inside or outside of the valid area. If the point is invalid, the corresponding row of the geometry matrix will be filled with zero. For example, if the first point of Fig. 2 is invalid ($p_1 = 0$), the rows of the geometry matrix corresponding to g_{x1} and g_{y1} should all be zero, and the like.

To realize the above revise, it is expected to use the matrix calculation and then, the mask matrix should have the same size of the geometry matrix A with $2n^2 \times n^2$. Thus, the expanded mask matrix may be expressed as

$$M = \begin{bmatrix} p_1 & \cdots & p_1 & \cdots & p_1 \\ \vdots & \ddots & \vdots & \ddots & \vdots \\ p_{n^2} & \cdots & p_{n^2} & \cdots & p_{n^2} \\ p_1 & \cdots & p_1 & \cdots & p_1 \\ \vdots & \vdots & \vdots & \vdots & \vdots \\ p_{n^2} & \cdots & p_{n^2} & \cdots & p_{n^2} \end{bmatrix}_{2n^2 \times n^2}. \tag{6}$$

Then the revised geometry matrix A_M can be written as

$$A_M = A \cdot M. \tag{7}$$

The reconstructed wave-front can be calculated by

$$\Phi = A_M{}^{+}G \tag{8}$$

According to the measured light spot distribution of S–H WFS, the mask matrix can be easily acquired. Furthermore, the slope matrix G can be obtained with the measured slope data. Therefore, the estimated wave-front can be calculated by Eq. (8).

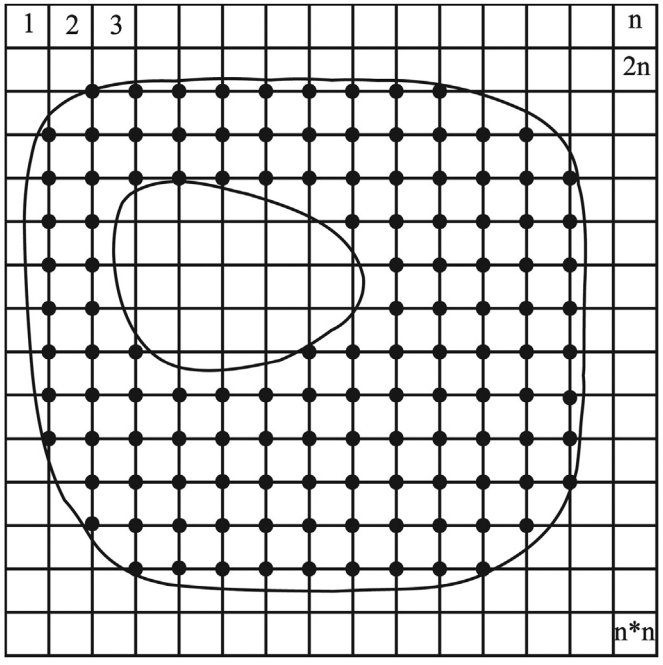

Fig. 2. Demonstration of the arbitrary shape pupil.

3. Wave-front reconstruction for annular pupil

3.1. Original wave-front

To simulate the wave-front reconstruction, an original wave-front and the slope data should be achieved firstly. As the aperture of the reflective telescope always has central obstruction, an annular wave-front is reconstructed firstly. An 50% central obstruction wave-front with the magnitude of 5λ ($\lambda = 780$ nm) is produced with the size of 420×420 as shown in Fig. 3(a). Assuming a 21×21 sub-region data corresponds to a sub-aperture of the S–H WFS, the slope data of a sub-aperture can be obtained by solving the average gradient of the corresponding sub-region. Thus, the slope matrix G can be acquired and its size is 20×20. Furthermore, the revised geometry matrix A_M can also be achieved according to the annular shape information. To calculate the reconstructed wave-front error conveniently, the original wave-front is reduced to 20×20 points (Fig. 3(b)) and each phase data is obtained by averaging the 21×21 phase data among a sub-region.

3.2. Reconstruction results

The reconstructed wave-front and the reconstruction error are shown in Fig. 4(a) and (b) respectively. To do the comparison, the Gerchberg-type iterative linear LS-based algorithm [14] is also

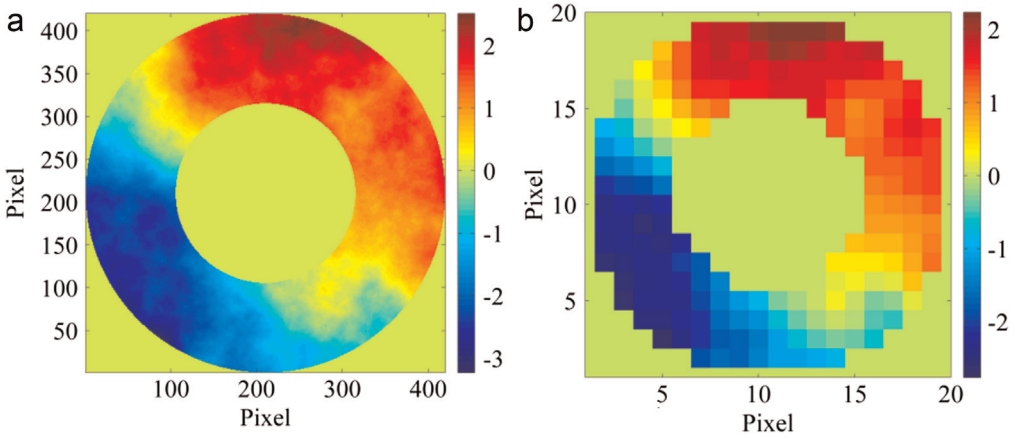

Fig. 3. Original wave-front: (a) produced with 420×420 points; and (b) reduced original wave-front with 20×20 points.

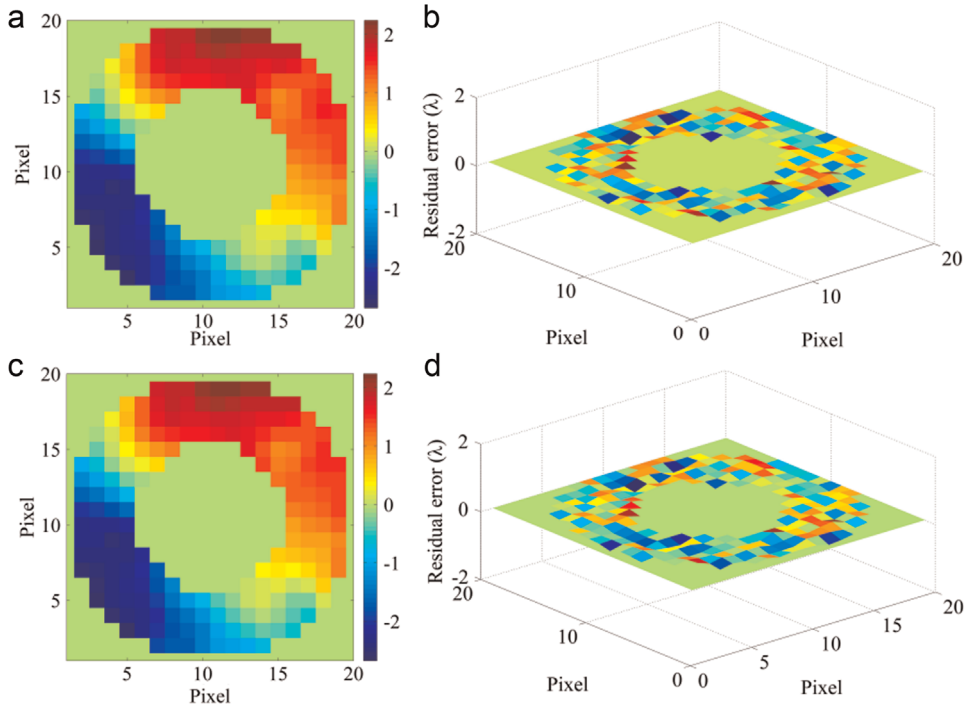

Fig. 4. Reconstruction of the annular wave-front: (a) reconstructed wave-front with proposed method; (b) residual of proposed; (c) reconstructed wave-front with iterative method; and (d) residual of iterative method.

utilized to reconstruct the wave-front in the paper. The annular wave-front shown in Fig. 4(c) is reconstructed with iterative LS-based method and Fig. 4(d) is the reconstruction error. It can be seen that, for both methods, the reconstructed wave-fronts are very close to the original wave-front. The reconstruction errors are calculated as shown in Fig. 5. It indicates that, for proposed method, the root mean square (RMS) value of the reconstruction error is 0.045λ. To the iterative LS-based method, the reconstruction error is firstly decreased and then the reconstruction error approaches a constant while the iteration times more than 12. With iteration times of 18, the reconstruction error is down to 0.045λ, which is the same as that of our method. It illustrates that the reconstruction accuracy of our method is as good as that of the iterative LS-based method.

The reconstruction time is also considered for two methods. A computer with the Inter Core(TM) i3-530 2.93 GHz and the memory of 2GB is selected to perform the computation. The reconstruction time is shown in Fig. 6 for two methods. It can be seen that the calculation time of our method is 1.2 s. For the

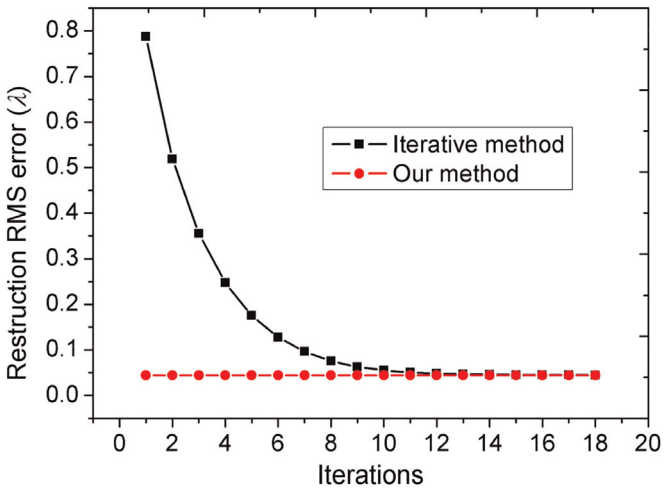

Fig. 5. Reconstruction RMS error for the annular wave-front.

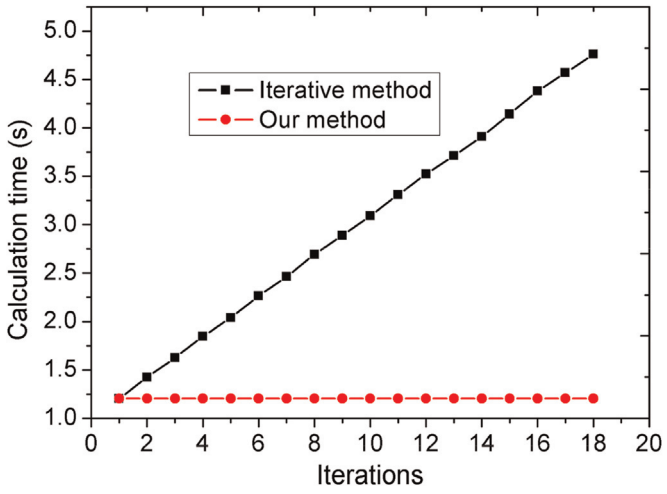

Fig. 6. Reconstruction time for the annular wave-front.

iteration method, the calculation time is proportional to the iteration times and 4.8 s is consumed with the iteration times of 18. Therefore, while the same reconstruction accuracy is achieved, the calculation time is reduced 3 times with proposed method. Then, we can say that the reconstruction speed is greatly improved.

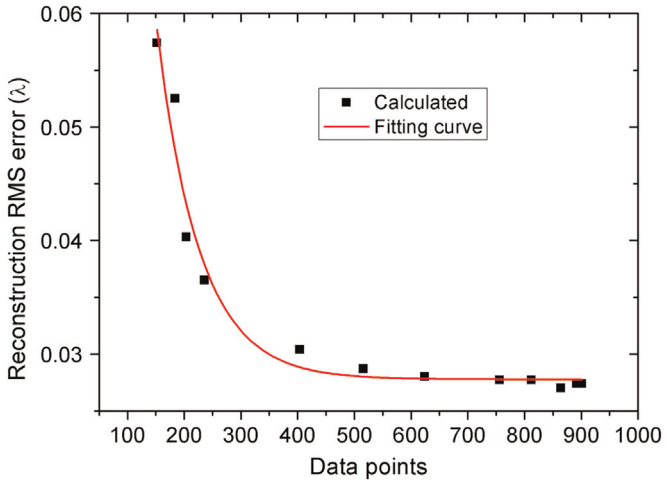

Fig. 7. Reconstruction RMS error as a function of slope data points.

3.3. Effect of the number of slope data on the reconstruction error

To investigate the effect of the slope data points, the central obstruction of the wave-front is changed to obtain different slope data points. The reconstruction error as a function of the slope data points is shown in Fig. 7. The real line is the fitting curve with following formula:

$$y = A \exp(-x/t) + y_0. \tag{9}$$

The fitting results show that, A is 0.23, t is 75.2, and y_0 is 0.028. It is shown that, with the increase of the slope data points, the reconstruction error drastically decreases firstly and then, goes to a constant. Furthermore, the reconstruction error is almost the same while the data points more than 600. Consequently, 600 data points is sufficient for the reconstruction of this wave-front.

3.4. Effects of wave-front magnitude on the reconstruction error

Without loss of generality, an annular wave-front with different magnitudes is reconstructed with iterative LS-based algorithm and our method respectively. The reconstructed wave-front error is calculated as shown in Fig. 8. It is shown that the reconstruction error is proportional to the wave-front magnitude for both methods. Furthermore, for larger wave-front magnitude, the reconstruction error of our method is fewer than that of the iterative LS-based method and the difference of the reconstruction error is shown in Fig. 8(b). This demonstrates that the reconstruction accuracy of our method is a little better than the iteration method for larger wave-front magnitude.

The above results are obtained with the same spatial sample points. As the spatial sample frequency will be decreased with the increase of the wave-front magnitude, we think that the increased wave-front reconstruction error is possibly caused by the low spatial sample frequency. To valid this, the wave-fronts are reconstructed with different magnitude and the same spatial sample frequency. The spatial sample frequency is defined as

$$S_R = \frac{PV_w}{n} \tag{10}$$

where PV_w is the wave-front magnitude and the unit is λ, n is the sample points along one dimension shown in Fig. 2. The spatial sample frequency of 0.1 is selected to do the calculation and the reconstructed result is shown in Fig. 9. It is shown that the reconstruction RMS error is almost the same with different wave-front magnitude. Consequently, the reconstruction accuracy is related to the spatial sample frequency, but not the wave-front magnitude.

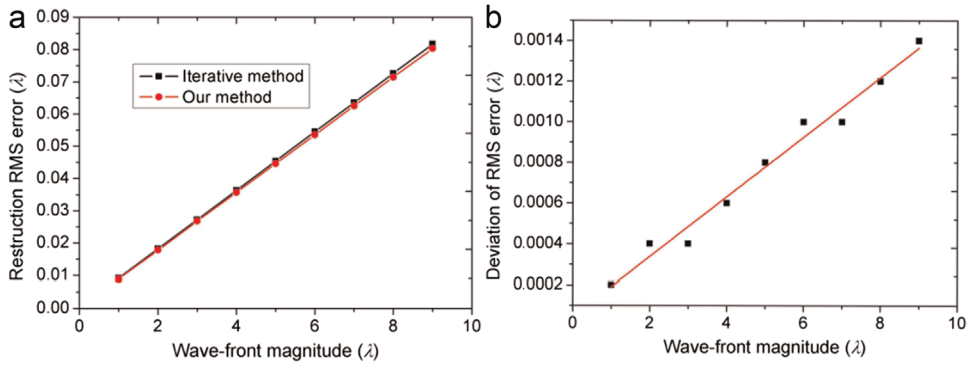

Fig. 8. Wave-front reconstruction with different magnitude: (a) reconstruction RMS error; and (b) deviation of RMS error.

4. Wave-front reconstruction for arbitrary shape

To validate our method, an arbitrary wave-front with the magnitude of 5λ is produced as shown in Fig. 10(a) and its reduced original wave-front is shown in Fig. 10(b). Then, the wave-front is reconstructed with iterative LS-based and our methods respectively and the reconstruction wave-fronts are shown in Fig. 10 (c) and (d). The calculated results show that the reconstruction error of the proposed method is 0.05λ, which is the same as that of the iterative LS-based algorithm with 18 iterations.

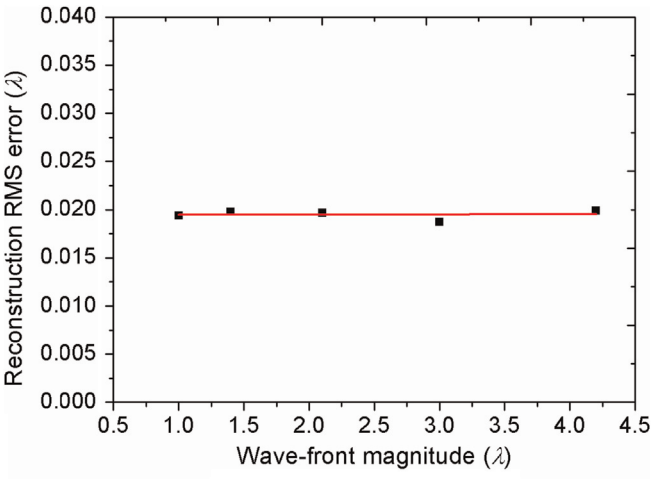

Fig. 9. Wave-front reconstruction error as a function of the wave-front magnitude with the spatial sample frequency of 0.1.

5. Experiment

A S-H WFS (Moscow State University) with 20 × 20 microlens array, 1 kHz frame frequency, and 4.2 mm aperture is chosen to measure the wave-front and the slope data. The measured wave-front, which is produced with 65 Zernike modes, is utilized as the original wave-front. The light spot array and the annular measured wave-front are shown in Fig. 11(a) and (b) respectively. To compare with the simulated results, the magnitude of the measured wave-front changes from 2λ–9λ approximately by changing the position of the point light source. The reconstruction errors as a function of the wave-front magnitude are shown in Fig. 12 for iterative LS-based and our methods respectively. It can be seen that, as the sample point of the S–H WFS is a constant, the reconstruction error changes as a linear function of the wave-front magnitude for both methods. This experimental result is similar to the simulated results as shown in Fig. 8. To the proposed method, the reconstruction error is closer to the simulated result; but the reconstruction error of the iterative method is a little larger than the simulated result. This phenomenon is possibly caused by detection noise of the S–H WFS. In any case, the tendency of experimental result is similar to that of the simulation. Consequently, we may say that the proposed method is valid for zonal wave-front reconstruction.

6. Conclusions

A shape based wave-front reconstruction method is demonstrated to reduce the time delay caused by the iteration algorithm. Firstly, the shape based LS method is established by revising the geometry matrix. Secondly, an annular wave-front with the

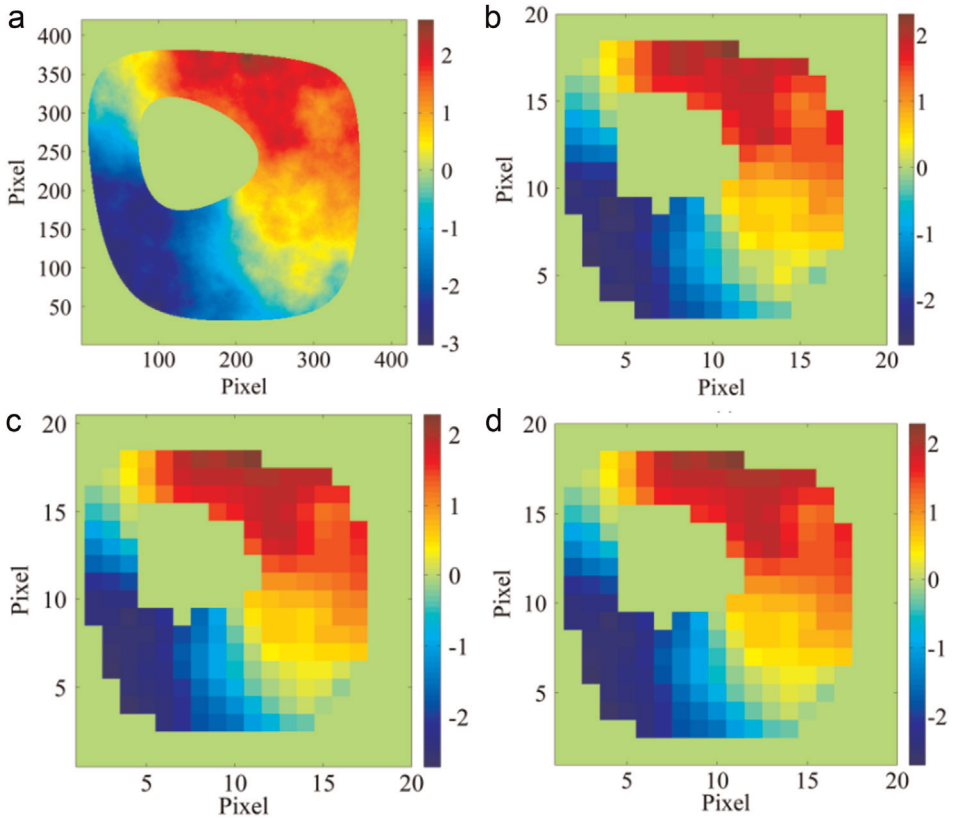

Fig. 10. Arbitrary wave-front reconstruction: (a) original wave-front; (b) reduced original wave-front; (c) reconstructed wave-front with our method; and (d) reconstructed wave-front with iterative LS-based method.

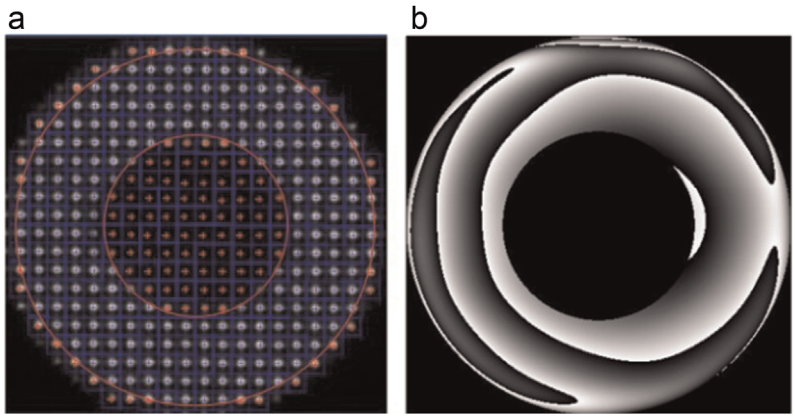

Fig. 11. Measured results of S–H WFS: (a) light spots; and (b) annular wave-front.

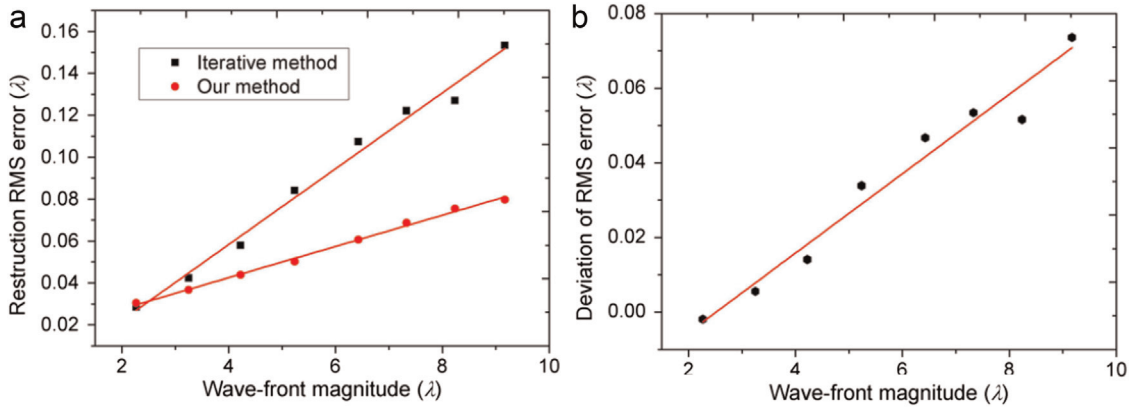

Fig. 12. Wave-front reconstruction with measured slope data, the real line is the linear fitting result: (a) reconstruction RMS error; and (b) deviation of RMS error.

magnitude of 5λ is reconstructed with the proposed method and the iterative LS-based algorithm respectively. The reconstruction error of our method is 0.045λ, which is the same as the iterative method with 18 iterations. However, the calculation time of proposed method is 3 times less than that of the iterative LS-based algorithm. Thirdly, the effect of the slope data points on the reconstruction error is considered. The simulated results show that the reconstruction error drastically decreases firstly and then, goes to a constant with the increase of the slope data points. Furthermore, the reconstruction error is almost the same while the data points more than 600. Moreover, the influence of the wave-front magnitude on the reconstruction error is investigated. It is shown that, with the same spatial sample frequency, the wave-front reconstruction accuracy has no relation with the wave-front magnitude. At last, an annular wave-front is reconstructed by using the slope data measured by a S–H WFS. The experimental results indicate that the reconstruction error is similar to that of the simulated results.

In a word, with the shape based LS method, the arbitrary shape wave-front can be reconstructed with high accuracy and low time consumption. Although only the Southwell model is considered in the paper, the proposed method can also be applied to the Hudgin and Fried models. This work is helpful for zonal wave-front reconstruction of arbitrary shape pupil.

Acknowledgments

This work is supported by the National Natural Science Foundation of China (11174274, 11174279).

References

[1] R.J. Noll, J. Opt. Soc. Am. 66 (1976) 207–211.
[2] Q. Zhang, W.H. Jiang, B. Xu, Opto-Electron. Eng. 25 (1998) 16–20, in Chinese.
[3] D.L. Fried, J. Opt. Soc. Am. 67 (1977) 370–375.
[4] W.H. Southwell, J. Opt. Soc. Am. 70 (1980) 998–1006.
[5] R.H. Hudgin, J. Opt. Soc. Am. 67 (1977) 375–378.
[6] K. Freischlad, C.L. Koliopoulos, Proc. SPIE 551 (1985) 74–80.
[7] S.W. Bahk, Opt. Lett. 33 (2008) 1321–1323.
[8] W.Y. Zou, Zh.Ch. Zhang, Appl. Opt. 39 (2000) 250–268.
[9] S.W. Bahk, Opt. Express 19 (2011) 18997–19014.
[10] L.A. Poyneer, D.T. Gavel, J.M. Brase, J. Opt. Soc. Am. A 19 (2002) 2100–2111.
[11] Q. Zhang, W.H. Jiang, B. Xu, High Power Laser Part. Beams 10 (1998) 229–233, in Chinese.
[12] R.L. Frost, C.K. Rushforth, B.S. Baxter, Appl. Opt. 18 (1979) 2056–2061.
[13] D.G. Sha, J. Beijing Inst. Technol. 11 (1991) 74–79, in Chinese.
[14] W.Y. Zou, J.P. Rolland, J. Opt. Soc. Am. A 22 (2005) 938–951.
[15] F. Roddier, C. Roddier, Appl. Opt. 30 (1991) 1325–1327.
[16] W.Y. Zou, J.P. Rolland, J. Opt. Soc. Am. A 23 (2006) 2629–2638.
[17] R.Z. Zhou, Adaptive Optics, National Defense Industry Press, Beijing, 1996.
[18] R. Tyson, Principles of Adaptive Optics, CRC Press, USA, 2010.